Origin and intra-annual variability of vertical microplastic fluxes in Fram Strait, Arctic Ocean

Lisa Roscher [a,f,*], Eva-Maria Nöthig [b], Kirsten Fahl [c], Claudia Wekerle [d], Thomas Krumpen [e], Mario Hoppmann [d], Nadine Knüppel [b], Sebastian Primpke [a], Gunnar Gerdts [a], Melanie Bergmann [f]

[a] *Alfred Wegener Institute Helmholtz Centre for Polar and Marine Research, Shelf Sea System Ecology, Kurpromenade 201, 27498 Helgoland, Germany*
[b] *Alfred Wegener Institute Helmholtz Centre for Polar and Marine Research, Polar Biological Oceanography, Am Handelshafen 12, 27570 Bremerhaven, Germany*
[c] *Alfred Wegener Institute Helmholtz Centre for Polar and Marine Research, Marine Geology, Am Alten Hafen 26, 27568 Bremerhaven, Germany*
[d] *Alfred Wegener Institute Helmholtz Centre for Polar and Marine Research, Physical Oceanography, Klußmannstraße 3d, 27570 Bremerhaven, Germany*
[e] *Alfred Wegener Institute Helmholtz Centre for Polar and Marine Research, Sea Ice Physics, Klußmannstraße 3d, 27570 Bremerhaven, Germany*
[f] *Alfred Wegener Institute Helmholtz Centre for Polar and Marine Research, HGF-MPG Joint Research Group for Deep-Sea Ecology and Technology, Am Handelshafen 12, 27570 Bremerhaven, Germany*

HIGHLIGHTS

- Near-monthly analysis of microplastics in Fram Strait, Arctic over almost two years
- Microplastic fluxes ranged from 0 to 2.9 MP m^{-2} d^{-1}, ~80 % of the particles were < 50 μm.
- Parallel assessment of biogeochemical and physical variables
- Backward and forward simulations of particle trajectories were computed.
- Backtracking of sea-ice revealed potential source regions.

GRAPHICAL ABSTRACT
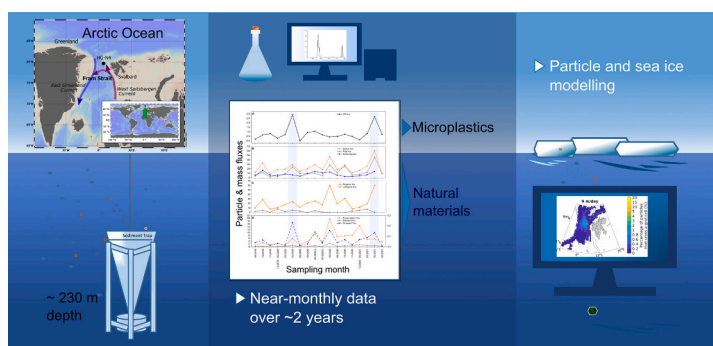
ARTICLE INFO

Editor: Dimitra A Lambropoulou

ABSTRACT

Microplastic (MP) pollution has reached the remotest areas of the globe, including the polar regions. In the Arctic Ocean, MPs have been detected in ice, snow, water, sediment, and biota, but their temporal dynamics remain poorly understood. To better understand the transport pathways and drivers of MP pollution in this fragile environment, this study aims to assess MPs ($\geq$ 11 μm) in sediment trap samples collected at the HAUSGARTEN observatory (Fram Strait) from September 2019 to July 2021. MP fluxes determined by μ-Fourier transform infrared (FTIR) imaging ranged from 0 to 2.9 MP m^{-2} d^{-1}, peaking in April 2020 and April 2021, with all detected MPs being <300 μm in size. There was no strong correlation between MPs and any of the recorded biogeochemical and physical variables, as each MP flux event was associated with different variables such as

* Corresponding author at: Alfred Wegener Institute Helmholtz Centre for Polar and Marine Research, Shelf Sea System Ecology, Kurpromenade 201, 27498 Helgoland, Germany.

E-mail address: lisa.roscher@awi.de (L. Roscher).

biogenic matter, sea ice concentration, or origin. By providing time series data over 21 months, this study provides a baseline for future MP flux assessments in Fram Strait, Arctic.

1. Introduction

Plastic pollution has spread in ecosystems around the globe (Allen et al., 2022; Tekman et al., 2022). In the Arctic, earliest records of plastic debris date back to 1957 from a Continuous Plankton Recorder (Ostle et al., 2019). More recently, seafloor images taken between 2004 and 2017 at the Long Term Ecological Research (LTER) observatory HAUSGARTEN in the Arctic showed almost a sevenfold increase in marine debris (Parga Martínez et al., 2020). Elevated shares of small-sized plastics indicated a fragmentation of larger plastic items, which may also include microplastics (plastics ≤5 mm; MPs). MPs are known to be ingested by organisms of various trophic levels and groups (Miller et al., 2020; Wang et al., 2021a), and can have adverse effects on organisms (Tekman et al., 2022). In the Arctic, MPs were recorded in benthic invertebrates (Fang et al., 2021), seabirds (Poon et al., 2017), fish (Morgana et al., 2018) or zooplankton crustaceans (Botterell et al., 2022) among other biota (Collard and Ask, 2021). To better understand general MP distribution patterns and pollution levels (and thus the potential exposure of biota), it is crucial to generate detailed data on MP pollution, especially in fragile ecosystems such as the polar regions.

For example, in past studies, various compartments in the Arctic were shown to be polluted with MPs. In sediment samples from the HAUSGARTEN observatory in the Fram Strait, very high concentrations of MPs were found (Bergmann et al., 2017; Tekman et al., 2020). Furthermore, Lusher et al. (2015) recorded MPs in the majority (> 90 %)

of surface and sub-surface water samples taken south and south-west of Svalbard in 2014. Further studies in Arctic waters were undertaken in the following years, e.g. in subsurface waters off Northeast Greenland (Morgana et al., 2018) or the Arctic Central Basin (Kanhai et al., 2018). In addition to water and sediment samples (Bergmann et al., 2017, Tekman et al., 2020), high concentrations of MPs have also been detected in Arctic snow (Bergmann et al., 2019; Rosso et al., 2024) and sea ice (Obbard et al., 2014; Peeken et al., 2018), demonstrating the ubiquity of MP pollution in the Arctic (Bergmann et al., 2022). To date, most MP studies are based on short-term assessments with a low temporal resolution. However, high-resolution time series data are needed to understand distribution patterns and the environmental factors driving them. Reineccius and Waniek (2022) studied MP fluxes in the subtropical North East Atlantic over 12 years, recording seasonality in some polymer types as well as a relationship with airborne minerals. In the Arctic, previous studies suggested that MPs could be linked to organic matter proxies and that increased abundances occur in proximity to the marginal ice zone (MIZ) (Bergmann et al., 2017; Tekman et al., 2020), pointing to sea ice as an important transport vector (Peeken et al., 2018). High concentrations of MPs were also recorded in the ice-associated alga *Melosira arctica* whose heavy aggregates could facilitate a rapid vertical transport of entrained MPs to the deep seafloor after ice melt (Bergmann et al., 2023). Generally speaking, very little is known about the temporal variability of MPs in the marine environment, even less so in the Arctic Ocean. The aim of this study is thus to link
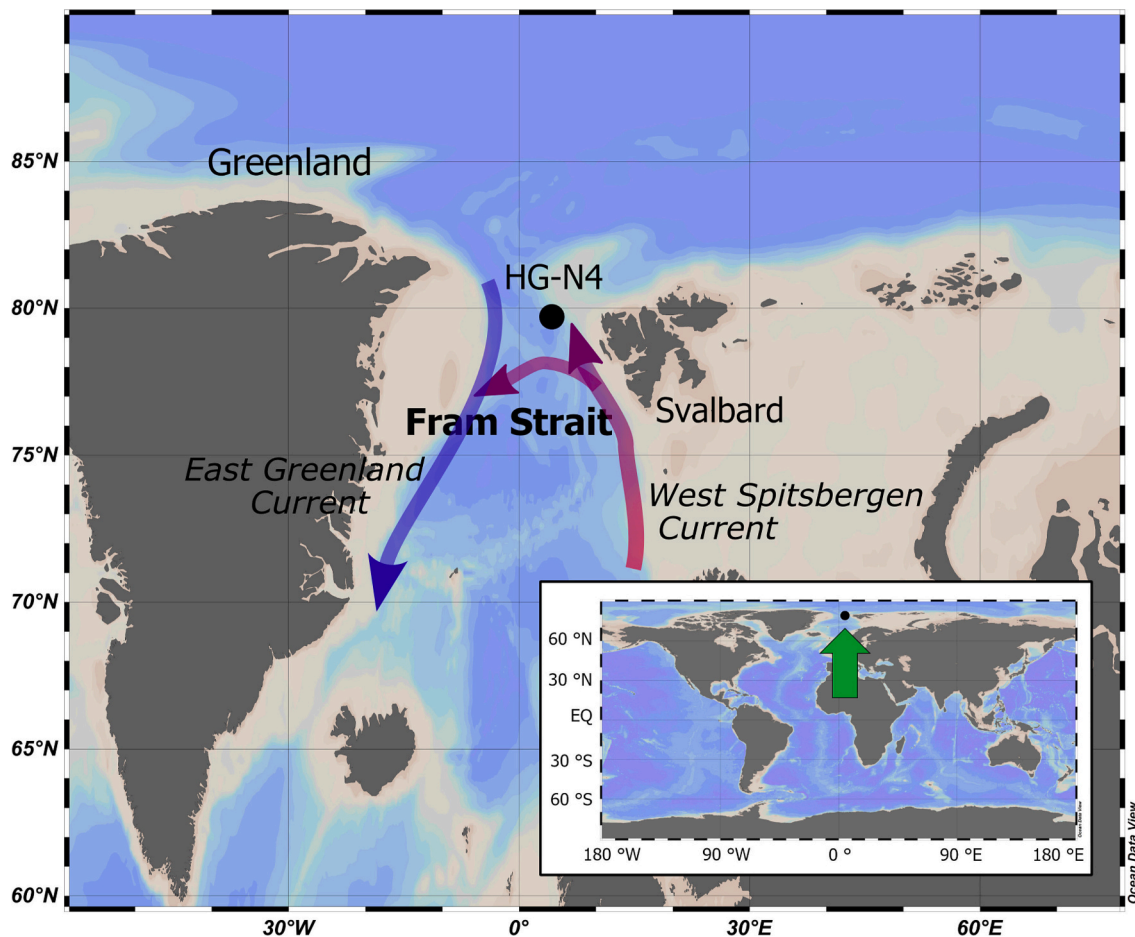

Fig. 1. Overview of sampling site. The map shows the location of the HAUSGARTEN station HG-N4 in Fram Strait, Arctic.

biogeochemical and physical variables with MP abundances and characteristics at a high temporal resolution at a sampling station located at the HAUSGARTEN observatory in Fram Strait (Fig. 1), to answer the following questions:

(a) Do MP fluxes vary over near-monthly time scales, and is there a link to biogeochemical and physical variables including natural matter fluxes and sea ice concentrations?
(b) Do polymer compositions and particle sizes vary over time?
(c) What are the past and future pathways of MPs?

To answer these questions, we quantified MPs in 18 sediment trap samples collected from September 2019 – May 2021 as well as biogeochemical and physical variables. Using particle modelling and sea ice backtracking, we deduced likely trajectories. This allowed us to gain new insights into MP pollution and the underlying biogeochemical and physical variables, as well as the potential fate of MP particles present in this region.

2. Materials and methods

2.1. Experimental design

To assess temporal variability in MP fluxes in Fram Strait, the deepest gateway to the Arctic Ocean, a sediment trap was deployed in the water column for 21 months (September 2019 to July 2021). We analysed MP data and underlying biogeochemical as well as physical parameters to evaluate potential transport scenarios using modelling approaches, including predicted particle trajectories and sea ice backtracking. The following sections will provide details on the respective methods, including sampling, sample processing, analyses of MPs and environmental parameters, along with methods used for model-based analyses and statistics.

2.2. Study area

The study site is part of the LTER observatory HAUSGARTEN in Fram Strait, which was established by the Alfred Wegener Institute, Helmholtz Centre for Polar and Marine Research in 1999, and currently comprises 21 sampling stations (Soltwedel et al., 2016). Stations located in the eastern part of HAUSGARTEN are strongly influenced by the inflow of Atlantic water via the West Spitsbergen Current, whereas the western part is characterized by the East Greenland Current, transporting cooler water from the central Arctic Ocean to the south (Fig. 1). Because of the hydrographic conditions, sea ice cover varies in the different parts of Fram Strait. The western part is predominantly ice-covered, whereas areas in the southeast are permanently ice-free, and areas in the central and northeastern part experience seasonal ice coverage (Soltwedel et al., 2016).

2.3. Sampling and initial sample processing

From 07 September 2019 to 01 July 2021, a cone-shaped automatic Kiel sediment trap (K/MT, sampling area ~0.5 m^2) was deployed in Fram Strait at a nominal depth of 223 m as part of mooring HG-N-FEVI-39 (79°44.348′N, 004°30.356′E, station HG-N4; Hoppmann et al. (2022)) to collect sinking MPs and natural material. The mooring was deployed during RV *Polarstern* expedition PS121 (Event ID: PS121_46-3; Metfies (2020)). The Kiel sediment trap was equipped with 20 collection cups, pre-programmed to sample from 15 to 91 days per cup. Collection cups (volume: 400 mL) contained seawater with HgCl$_2$ (0.14 % final solution) for sample preservation. The sediment trap was recovered during RV *Polarstern* expedition PS126 (EventID: PS126_18-8; Soltwedel (2021)), and samples were stored at 4 °C. A sample list is provided in Appendix A, Table A1. In the laboratory, we documented the height of sedimented material as well as the pH. A volume of 10 mL was sampled with a glass pipet, filtered with a syringe filter, and stored at 4 °C for nutrient salt analysis. Afterwards, we divided samples in half using a custom-made Folsom plankton splitter. Half of the sample was designated for the assessment of biogeochemical parameters of sinking particles. It was transferred back to the sample bottle, and stored at 4 °C until further analysis. The other half, used for MP analysis, was stored in 500 mL glass bottles at 4 °C until further treatment.

2.4. Assessment of biogeochemical and physical variables

Samples were split by a wet-splitting procedure (Bodungen et al., 1991). The assessment of biogeochemical parameters of sinking particles included the analysis of seston (total particulate matter, TPM), particulate organic matter (POM), total organic carbon (TOC), particulate organic carbon (POC), biogenic silica, CaCO$_3$ content, as well as biomarkers. Before splitting of samples, we manually removed swimmers >0.5 mm under a dissecting microscope at a magnification of 20 to 50. Sub-samples of the remaining material were filtered for the subsequent analyses of biogeochemical parameters (see above), and were performed as described by Bodungen et al. (1991). Subsamples for total sedimented matter flux (seston) measurements were filtered onto pre-weighed GF/F filters (nominal pore size: 0.7 μm; 25 mm ø, pre-combusted (500 °C, 4 h), rinsed with distilled water to remove salt, dried at 60 °C, and weighed. POM was then determined by burning (500 °C, 4 h), and weighing these filters again, with POM representing the difference between the seston and burned carbon. Subsamples for CaCO$_3$ measurements were also filtered onto another pre-weighed GF/F filter of the same size and treated like the seston filter, but soaked in 0.1 N HCl to remove inorganic CaCO$_3$, rinsed and dried at 60 °C, and weighed again, with the carbonate fraction representing the difference between the total particulate matter and dissolved CaCO$_3$. Subsamples for POC measurements were filtered onto pre-combusted GF/F filters (500 °C, 4 h), then soaked in 0.1 N HCl for removal of inorganic carbon and dried at 60 °C. POC measurements were conducted on a Carlo Erba CHN elemental analyser. Subsamples for bPSi measurements were filtered on cellulose acetate filters (pore size: 0.8 μm), processed using the wet-alkaline method (pre-treated at 85 °C, 12 h), and extracted at 85 °C for 2 h in a shaking water bath. The fraction of biogenic matter in the total particulate matter was calculated from: $2 \times POC + CaCO_3 + Opal$ (Opal = $2.1 \times bPSi$), with the lithogenic fraction representing the difference between the total particulate matter (seston) and the biogenic matter.

We also analysed subsamples for the presence of biomarkers (brassicasterol, sitosterol, dinosterol, and IP$_{25}$). Brassicasterol and dinosterol are indicative for marine input (Volkman, 1986), while sitosterol has been established as reliable indicator for terrigenous input (Huang and Meinschein, 1979). IP$_{25}$ (highly-branched isoprenoid (HBI) alkene with 25 carbon atoms) is derived from specific sea ice diatoms (Belt et al., 2007; Brown et al., 2014).

Brassicasterol (24-methylcholesta-5, 22E-dien-3β-ol), sitosterol (24-ethylcholest-5-en-3β-ol), dinosterol (4a-23,24-trimethyl-5a-cholest-22E-en-3β-ol) and IP$_{25}$ were extracted with dichlormethane/methanol (1:1, *v/v*) and dichlormethane using separating funnels. For quantification of the lipid compounds, the internal standards 7-hexylnonadecane, C36 n-alkane, nonadecanoic acid, and androstanol (5α-androstan-3β-ol) were added prior to further analytical steps. IP$_{25}$ and sterols were separated via open column chromatography (SiO$_2$) using n-hexane for the hydrocarbons and ethyl acetate/n-hexane (20:80 v/v) for sterols as eluent. The individual sterols were silylated with 500 μL BSTFA (bis-trimethylsilyl-trifluoroacet-amide) at 60 °C for 2 h. After extraction with hexane, analyses were carried out by gas chromatography–mass spectrometry (GC–MS) using an Agilent 6850 GC (30 m DB-1 MS column, 0.25 mm inner diameter, 0.25 μm film thickness) coupled to an Agilent 5975C VL mass selective detector with Helium as carrier gas. Individual compound identification was based on comparisons of their retention times with that of reference compounds and on comparisons of

their mass spectra with published data (Boon et al., 1979; Volkman, 1986; Belt et al., 2007). IP_{25} was quantified using its molecular ion *m/z* 350 in relation to the abundant fragment ion m/z 266 of 7-hexylnonade-cane and by means of an external calibration curve ($R^2 = 0.9989$) to balance the different responses of the used ions (Fahl and Stein, 2012). Brassicasterol, sitosterol, and dinosterol were quantified as trime-thylsilyl ethers using the molecular ions m/z 470, m/z 486, and m/z 500, respectively, in relation to the molecular ion m/z 348 of androstanol.

The above-mentioned parameters were converted to fluxes in the units mg and µg m^{-2} d^{-1} by dividing the measured mass values by the trap opening and the number of sampling days.

Furthermore, physical parameters such as seawater temperature, pressure, and ocean currents were recorded at hourly intervals using a Seaguard single-point current meter (Aanderaa, Norway) located close to the sediment trap at a nominal depth of 230 m. We calculated monthly averages of these parameters to determine the seasonal vari-ability of ocean current velocity and -direction, and to link them to the sediment trap data.

2.5. Sample preparation and analysis of microplastics

The subsample for MP analysis was firstly poured over a metal sieve of 500-µm mesh size to differentiate between large MP (L-MP, 500–5000 µm) and small MP (S-MP, <500 µm). Similar size fraction-ations have been performed in previous studies (Bergmann et al., 2017; Löder et al., 2017; Tekman et al., 2020), and enable subsequent chem-ical analyses in two different modes of Fourier Transform Infrared Spectroscopy (FTIR). The following sections explain the processing and analysis approaches used for both size fractions, as well as contamina-tion mitigation measures.

2.5.1. Small microplastics (S-MP, 11–500 µm)
The sample fraction >500 µm was returned into the glass bottles and stored at 4 °C until further handling. The fraction <500 µm was concentrated onto pre-weighed 15-µm stainless steel filters (GKD, Ger-many) using a glass filtration unit. When filters started to clog, they were changed, with 1–5 filters required per sample. Filters were dried (40 °C, 24 h) and weighed again to assess the dry weight of the sample material. To isolate putative MPs, we subjected these filters to the following treatment: After transfer into 150 mL glass beakers, 40 mL of a 10 % KOH solution (*w/v*) prepared with KOH pellets (VWR, Darmstadt, Ger-many) was added. A hotplate stirrer (IKA C-MAG HS control, Germany) was applied in combination with a polytetrafluoroethylene (PTFE) cage stirrer (Bola Beakerliner, PTFE, Omnilab Laborzentrum GmbH & Co. KG, Germany) (400 rpm, 40 °C, 12 h). After digestion, we concentrated the remaining sample material onto the same filter, rinsed it into a 100-mL glass bottle with MilliQ water, and stored it at 4 °C. To remove any re-sidual inorganic material denser than microplastics, a density separation step was performed. LST Fastfloat© (Polytungstates Europe, UK) was adjusted to a density of approx. 1.6 g cm^{-3} (range: 1.59 g cm^{-3}–1.61 g cm^{-3}) using a handheld density meter (model: Density2Go, Mettler-Toledo GmbH, Germany). Separation funnels (volume: 50 mL) were used, as described in Abel et al. (2022). The resulting sampling material was stored in MilliQ water in 100-mL glass bottles.

The sample fraction containing putative MPs was concentrated onto aluminium oxide filters (Anodisc©, Ø 25 mm, Whatman), commonly used for µFTIR analyses (Primpke et al., 2022). As the measurement of single aliquots and subsequent extrapolation might lead to over- or underestimation of MP numbers (Abel et al., 2021; Roscher et al., 2021), 100 % of the purified sample material was filtered onto 1–10 Anodisc filters and dried in a desiccator (Sicco, Bohlender GmbH, Germany) for 48 h in preparation for MP analysis. Measurements were performed using a Hyperion 3000 µ-FTIR microscope equipped with a Focal Plane Array (FPA) detector (64 × 64 detector elements), connected to a TENSOR 27 spectrometer (Bruker Optics GmbH, Germany). Before the

measurement, Anodisc filters were covered with a BaF_2 window (Primpke et al., 2019). Although this method is suitable for the analysis of MP fibres, we decided to exclude those, as no atmospheric blanks were collected on the ship so that fibre contamination cannot be ruled out. The measurement was performed in Bruker OPUS 8.5 (Bruker Op-tics GmbH), using the 3.5× IR objective, spectral resolution of 8 cm^{-1}, 32 co-added scans (background: 64 scans), and a spectral range of 3600–1250 cm^{-1}. Further settings were a Blackman-Harris 3-term apodization and a zero-filling factor of 2. A grid of 22 × 22 measure-ment fields was selected, which covered the entire relevant filter area.

Spectral data were first processed in Bruker OPUS (version 8.8.2.267), using a normalisation function (offset-correction), and exported in the ENVI file format (.hdr and .img). In the software siMPle (Primpke et al., 2020) (version 1.3.1 β, available upon request), spectral data were further processed: Pixels belonging to the PP edge of the Anodisc filter were removed, applying the in-built circular mask func-tion within the heat map function. The next step was the comparison of sample spectra to our in-house FTIR database in siMPle (Roscher et al., 2022), followed by automated data analysis within siMPle using the APA approach (Primpke et al., 2017). Final output data were .csv tables containing particle information including polymer type and size, as well as image files mapping the detected particles. During analyses, particle recognition was hampered for one sample (sampling month: March 2020, Anodisc 1) as one large putative polystyrene (PS) particle was recognized as 11 smaller ones. As both the heatmap function (Fig. A2 A) and visual observation showed the presence of a large item in this po-sition, spectra in between the assigned pixels were extracted and observed to be similar to the identified PS spectra of the adjacent assigned pixel (Fig. A2 B + C). We checked all relevant pixels in this area for their spectra, and if positively validated, added them using the 'Include pixel' function in siMPle (the resulting spectral map for the particle is shown in Fig. A3). MP numbers were corrected accordingly.

Results obtained for blank samples were subtracted from the sample results, and as samples were initially split into two halves, data were extrapolated to the whole sample. Particle numbers were converted into MP particle fluxes (in the following denoted as [MPs m^{-2} d^{-1}]) by dividing MP particle numbers by the sampling area of the sediment trap and the number of sampling days. In the cases where several Anodisc filters were used per sample (S-MP fraction), respective MP counts were summed up. Besides our database-related polymer categorisation, polymer types were assigned to the recently recommended polymer groups and size ranges (AMAP, 2021; Primpke et al., 2022) (Appendix C).

2.5.2. Large microplastics (L-MP, 500–5000 µm)
The sample material >500 µm was transferred into a glass bowl and screened for putative MPs with a stereomicroscope, based on the criteria presented in Norén (2007). Larger amphipods ('swimmers') were removed by tweezers and refrigerated in seawater for future MP assessments and the visual inspection of samples. Putative MPs were isolated, and their colour and shape were documented as previously recommended for Arctic monitoring (Lusher et al., 2020; Primpke et al., 2022) (Appendix B). One putative MP particle was measured by FTIR-ATR (Bruker Tensor 27 Sys-tem, Bruker Optics GmbH). Prior to the measurement, the particle was placed on the diamond crystal of the ATR unit and fixed with a clamp. Measurement settings in Bruker OPUS 7.5 were a spectral range of 400–4000 cm^{-1}, a resolution of 4 cm^{-1}, and 32 co-added scans (further settings: Blackman-Harris 3-term apodization, zero-filling factor: 2). Spectra were recorded in triplicates, converted to .dx files and polymer identification was performed in siMPle (version 1.1.β). Isolated putative MP fibres were analysed, but finally excluded from the results, as explained above.

2.5.3. Mitigation and assessment of contamination
Laboratory ware was made of glass or stainless steel, wherever possible. We rinsed all sampling containers thoroughly with MilliQ

water before usage. Seawater, KOH, LST Fastfloat, and ethanol were pre-filtered through glass fibre filters (Ø 47 mm, 0.7 μm pore size; VWR, Germany) or GTTP filters (Ø 47 mm, 1.2 μm pore size; Merck Millipore, Germany) to remove potential particle contamination. Whenever possible, sample processing was conducted under a fume hood or a laminar flow cabinet, and cotton lab coats were worn.

Blank samples were prepared to assess potential MP background contamination. Three respective container blanks were prepared to estimate the contamination from the PP collector cups containing the $HgCl_2$ – intoxicated seawater prepared before sampling. These collector cups had been deployed within the sediment traps but did not open during sampling, and therefore did not contain any sample material or secondary contamination. The content was filtered onto the 15-μm stainless steel filters (see above) and subsequently transferred onto Anodisc filters for μ-FTIR analysis. To account for contamination during sample processing, three procedural blanks were treated in the same way as the samples reflecting potential contamination from the laboratory equipment, used chemicals, and laboratory air. Average MP counts from container and laboratory blanks were summed up, and subtracted from the results of the environmental samples (subtraction per polymer type and size class) (Appendix C). This approach may represent an overestimation of the real contamination by the collector cups, as respective blanks were directly filtered and did not undergo processing steps and sample transfers. LOD/LOQ was assessed for the procedural blanks on polymer type level, with LOD calculated as the average number of particles plus 3 times the standard deviation, and LOQ as 3 times LOD (Vitali et al., 2024). Polymer clusters with counts below LOQ were marked in the results.

2.6. Particle tracking

We used the velocity field from an ocean-sea ice model to compute 3D particle trajectories starting from the station HG-N4 at 223 m depth. First, particles were traced backwards from the mooring site at 200 m depth to the surface of the ocean, revealing the origin of the particles. The trajectory computation thus stopped once particles reached the sea surface. In a second step, the particles were traced forward until they reached the seafloor, revealing the fate of the particles. The particle trajectories were determined with a Lagrangian particle-tracking algorithm (Wekerle et al., 2018), following Tekman et al. (2020). For both the forward and backward computation, three different sinking velocities (53 m d^{-1}, 27 m d^{-1}, and 9 m d^{-1}) were applied to account for different particle sizes (Wekerle et al., 2018; Tekman et al., 2020). The horizontal velocity fields with daily temporal resolution were taken from the ocean-sea ice model FESOM1.4 (Wekerle et al., 2017). The model configuration used in this study was optimized for the Fram Strait region, applying a high mesh resolution of 1 km in this area. It covers the period 1990–2018 and is forced with atmospheric re-analysis data from Era-interim (Dee et al., 2011). For the backward trajectories, particles were released once per day during the period 2010–2018 (resulting in a total of 3285 trajectories), whereas in the forward trajectory, particles were released once per day during the period 2010–2017 (2920 trajectories). We used a time step of 1 h for the trajectory calculation, yielding hourly positions. Probability maps of the particle distributions were generated by counting the number of particles that reached the surface, revealing the catchment area, and by counting the visit of a particle as it crossed a grid cell, revealing the fate of the particles. Catchments of particles are named in the following as catchment area I, II, and III, referring to the three different underlying sinking velocities (53 m d^{-1}, 27 m d^{-1}, and 9 m d^{-1}).

2.7. Assessment of sea ice concentrations and sea ice origins

We extracted and contextualised satellite-derived ice concentrations within the modelled particle catchment areas I-III (Section 2.6), along-side MP fluxes and environmental parameters. The sea ice concentration product utilised in this study is sourced from the Center for Satellite Exploitation and Research (CERSAT) and relies on 85 GHz SSM/I brightness temperatures, employing the ARTIST Sea Ice (ASI) algorithm. This product is available on a 12.5 km × 12.5 km grid (Ezraty et al., 2007).

To ascertain the age, trajectory, and origin of sea ice within the catchment area, we traced a central position backward in time using the OSI-405-c sea ice motion product from the Ocean and Sea Ice Satellite Application Facility (OSISAF, Lavergne (2016)). In brief, the sea ice tracking approach works as follows: An ice parcel is traced backward in time on a weekly basis. Tracking is stopped if a) the ice hits the coastline or fast ice edge, or b) the ice concentration at a particular location drops below 20 % and we assume the ice is forming. For a more detailed method description and discussion of uncertainties, we refer to Krumpen et al. (2019) and Krumpen et al. (2020).

2.8. Statistical analysis

For the creation of graphs and descriptive statistics, we used the softwares Matlab, Statistica and OriginPro2021b. As data of most variables were not normally distributed, Spearman's rank order correlations were performed. MP polymer diversity was expressed as Shannon-Wiener-Index (H′), using the software Primer-e 7 (Clarke and Gorley, 2015). The sea ice cover in the catchment areas and the origin of the ice were calculated using IDL routines (NV5 Geospatial). The overview map showing the location of the sampling station was created using the software Ocean Data View (Schlitzer, 2022).

3. Results

3.1. Microplastic fluxes in the context of biogeochemical and physical variables

Microplastics were only detected in the sample fraction <500 μm (S-MP), as all visually pre-sorted items from the >500 μm fraction were chemically identified as natural materials (Appendix B). Total numbers of MP particles per sample varied between 0 and 18 after blank correction (Appendix C). The average MP flux over the entire sampling period was 0.82 ± 0.78 MPs m^{-2} d^{-1}, with the highest values in April 2020 and in April 2021 (2.9 and 2.7 MPs m^{-2} d^{-1}, respectively) (Fig. 2A), and no MP flux was recorded for May 2020.

The high MP flux in April 2021 coincided with increased seston values of 60.6 mg m^{-2} d^{-1} (Fig. 2B; Appendix D) (average: 23.3 ± 13.4 mg m^{-2} d^{-1}). Particulate organic matter (POM) contributed strongly to the seston load in April and October 2020, as well as in April 2021. The patterns of carbonate fluxes were less distinct, with only slightly increased values in October 2019, July 2020 and April 2021 (Fig. 2B). Spearman's rank order correlations showed no significant correlation of MPs with seston, POM, or carbonate fluxes (Table A2), but a weak positive correlation with biogenic fluxes ($r_s = 0.48$, $p < 0.05$). The latter amounted to 22.5 ± 15.8 mg m^{-2} d^{-1}, whereas lithogenic fluxes were at 2.7 ± 2.6 mg m^{-2} d^{-1} (Fig. 2C).

Although the maximum dinosterol flux (0.2 μg m^{-2} d^{-1}), indicative for marine input, coincided with the first MP peak in April 2020, no significant correlation was found. Also, sitosterol and brassicasterol did not significantly correlate with MP fluxes. The same was the case for the biomarker IP_{25}, reflecting the presence of certain Arctic sea ice diatoms (Belt et al., 2007), which showed fluxes between 0 and 0.9 μg m^{-2} d^{-1} (Fig. 2E). It was mainly recorded in the first study months (peaking in October 2019 and March 2020), and mostly absent from April 2020 onward. Sea ice concentrations determined for the modelled catchment areas I-III (cf. Section 2.6) were between 25 and 35 % in autumn 2019, and mostly at 50–70 % between March and June 2020 (Fig. 2E). The high sea ice concentrations and subsequent decline in spring 2020 coincided with the MP peak in April 2020. From June 2020 on, sea ice concentrations decreased, with consistently low values ≤15 %, until
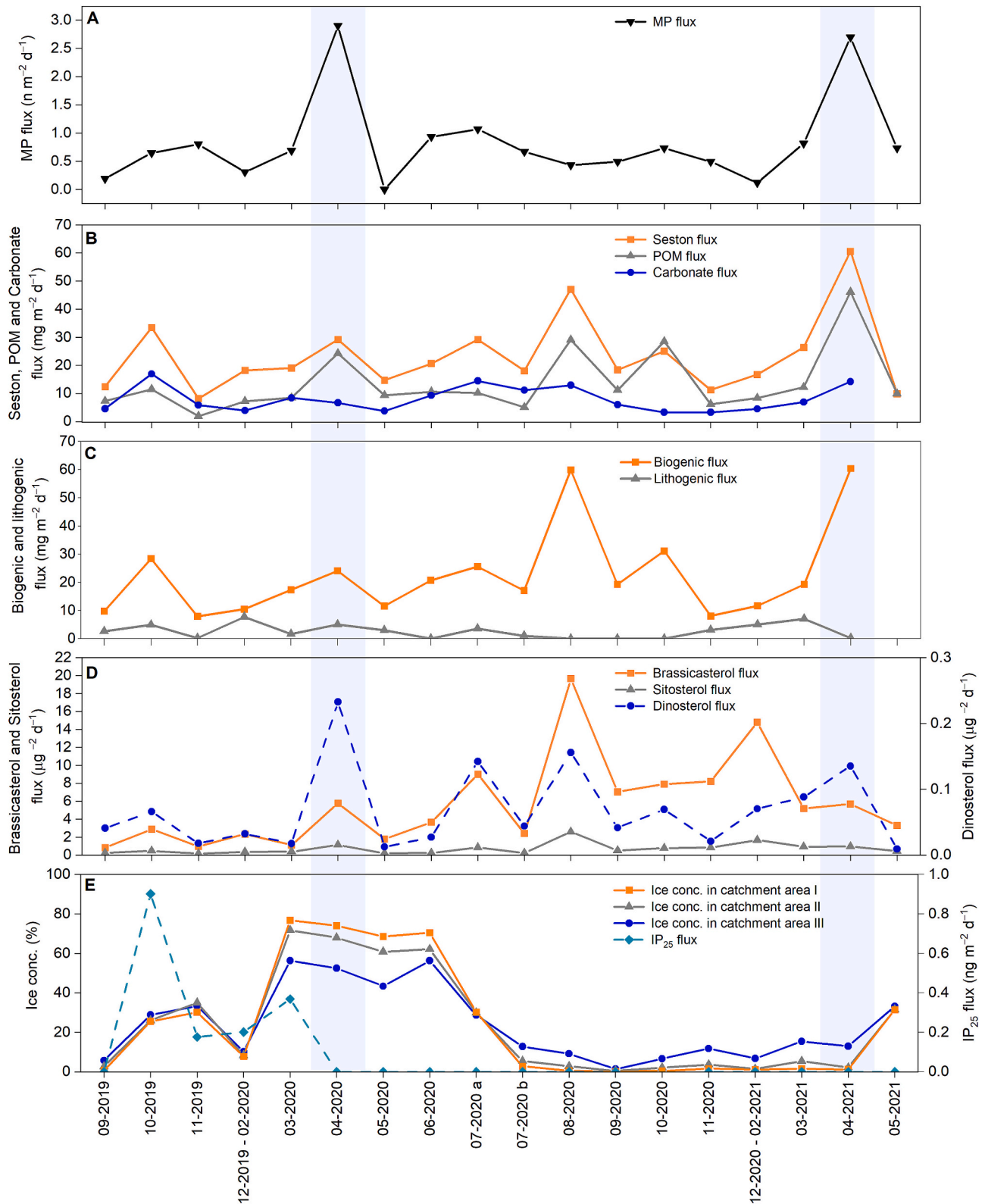
Fig. 2. MP fluxes, biogeochemical variables and sea ice concentrations in sediment trap samples taken between September 2019 and May 2021 in Fram Strait. (A) MP flux, (B) suspended matter flux (seston, POM, and carbonate), (C) biogenic and lithogenic flux, (D) brassicasterol, sitosterol, and dinosterol flux, (E) sea ice concentrations (monthly average) and IP_{25} flux from September 2019 – May 2021. Sea ice concentrations are provided for three different potential catchment areas of particles, based on different particle sinking velocities in the FESOM model (catchment I: 53 m d^{-1}, catchment II: 27 m d^{-1}, catchment III: 9 m d^{-1}). Abbreviations: MP: microplastic; POM: particulate organic matter; IP_{25}: ice algae proxy; conc.: concentration. Months highlighted in blue indicate maximum MP flux values. Note that the x-axis only displays an approximation to temporal continuity over the sampling period, as the number of sampling days varied (cf. Table A1).

they increased again towards the end of the study period in May 2021.

The current velocity varied strongly throughout the sampling period, with monthly averages being lowest in July 2020 (0.08 ± 0.03 m s^{-1}) and highest in February 2021 (0.26 ± 0.08 m s^{-1}). Current directions showed a strong intra-monthly variability, with the exception of April 2021, where high-velocity currents were mainly directed south-eastwards (Fig. A1). Seawater temperatures were at 2.8 ± 0.5 °C, with a minimum monthly average of 2.0 ± 0.5 °C (April 2021) and a maximum of 3.4 ± 0.2 °C (October 2019). The average depth of the sediment trap over the whole study period was 252 ± 37 m, with variabilities caused by changing current velocities and subsequent sinking of the instruments.

3.2. Microplastic polymer compositions and size distributions

The number of different polymer types detected ranged from 0 to 7 (Fig. 3A), and was significantly positively correlated with total particle numbers ($r_s = 0.85$, $p < 0.05$). The highest polymer diversity was recorded in the April 2021 sample (Shannon H′ = 1.8), followed by the sample collected in December 2019 – February 2020 (H′ = 1.7) and April 2020 (H′ = 1.6). Common polymer types were polyamide (PA) and polyvinyl chloride (PVC), which were present in 72 % and 50 % of the 18 samples and accounted for 25 % and 21 % of all detected MPs. Polyester (PEST) was the third most abundant polymer type (12 %). Rarer polymer groups included chemically modified cellulose (CMC), and polyoxymethylene, which were only found in 6 % of the samples each. Polystyrene (PS) was only present from November 2019 to March 2020, and chlorinated polyethylene (CPE) both in October 2019 and October 2020. In the April 2020 peak, the polymer composition was dominated by PVC, followed by PA, while the April 2021 peak had a slightly higher polymer diversity, with PE showing the highest flux. It is noted that LOD/LOQs assessed for procedural blanks showed that counts for polypropylene (PP), PA, CMC, and acrylates/polyurethanes/varnish (APV) in samples were lower than respective LOQs, thus for these polymer types an influence of contamination cannot be completely ruled out. Contamination with PP could be assigned to the collector cups to a
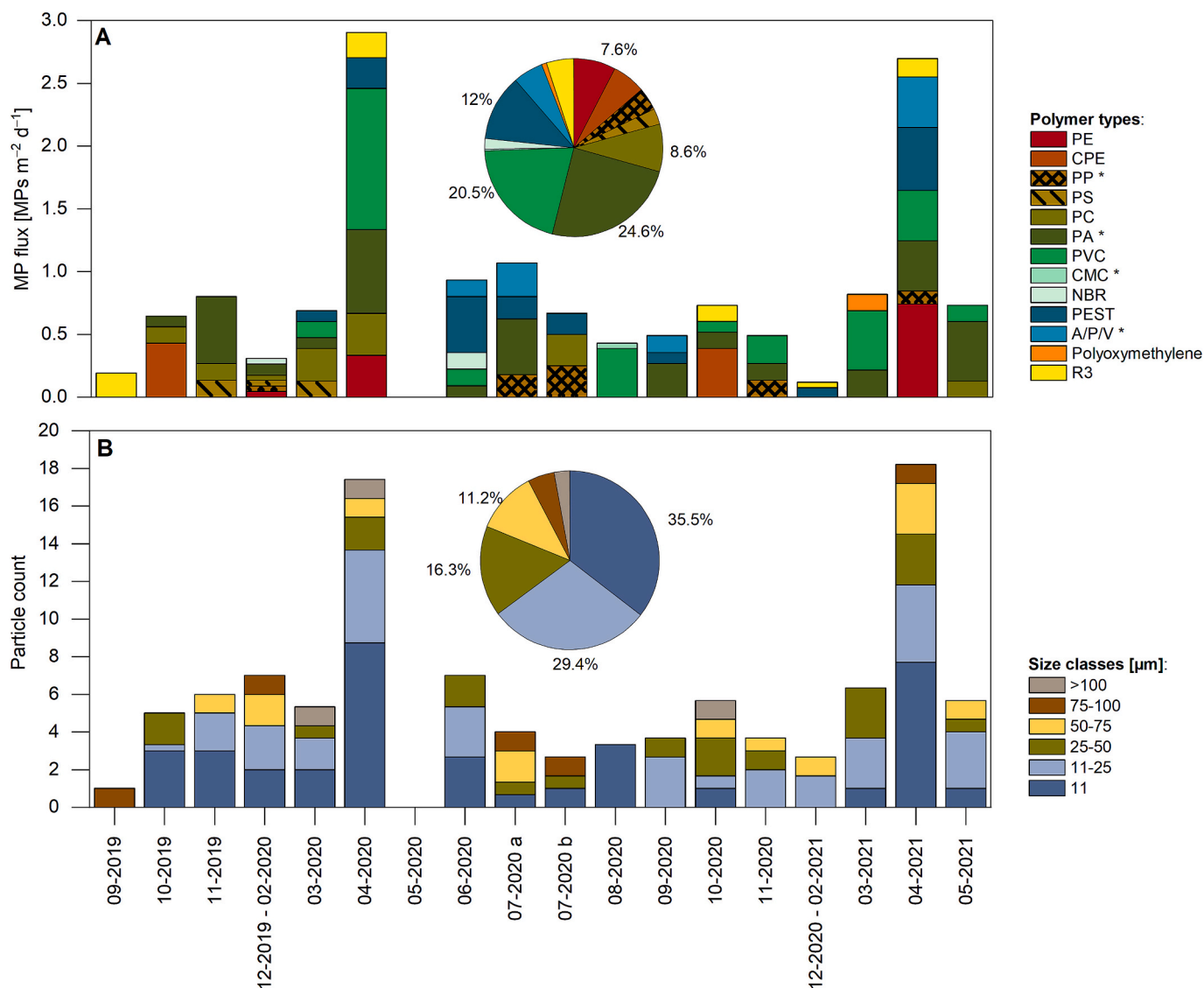

Fig. 3. MP fluxes and particle characteristics. (A) MP flux per month and contribution of different MP polymer clusters (pie chart: overall polymer composition), (B) Particle count per month (after blank-correction), and size class distribution (pie chart: overall size class distribution) in [μm]. The analysed size range was 11–5000 μm, with all detected MP particles being <300 μm. Polymer types marked with an asterisk exhibited counts below LOQ, and are potentially impacted by secondary contamination. Abbreviations: MP: Microplastics; PE: Polyethylene; CPE: Chlorinated polyethylene; PP: Polypropylene; PS: Polystyrene; PC: Polycarbonate; PA: Polyamide; PVC: Polyvinyl chloride; CMC: Chemically modified cellulose; NBR: Nitrile rubber, PEST: Polyester; A/P/V: Acrylates/polyurethanes/varnish; R3: Rubber type 3. Note that the x-axis only displays an approximation to temporal continuity over the sampling period, as the number of sampling days varied (cf. Table A1).

certain extent, with the three container blanks showing an average of 8 ± 6 particles.

All particles identified as MPs were smaller than 300 μm. The majority (35 %) was assigned to the smallest size class ≤11 μm (Fig. 3B). Clear temporal trends of size class distributions were not observed. The number of different size classes was significantly positively correlated with the number of detected particles per sample ($r_s = 0.76$, p < 0.05). As recommended by Primpke et al. (2022) in the context of standardised MP monitoring in the Arctic, MP results obtained in this study are also provided in the size classes >1 mm, 1 mm – 300 μm, and 300 μm to $LOD_{(size)} = 11$ μm, and polymers were grouped accordingly (Appendix C).

3.3. Potential past and future trajectories of particles

Backward particle trajectories reveal the catchment areas of MP detected at our study site (Fig. 4A). The size of the catchment area strongly depends on the assigned sinking speeds. In the case of fast sinking speeds of 53 m d^{-1}, MP particles originate from an area close to the study site. The average distance between the study site and the location where the particles reach the surface is 25 km, and the particles travel on average 36 km. In contrast, when a slow sinking speed of 9 m d^{-1} is imposed, the particles have a longer residence time in the water, resulting in longer trajectory path lengths (on average 198 km) and an increased distance to the study site (on average 94 km). In this case, most particles originate from the southeast, indicating that they have been carried with the West Spitsbergen Current, which transports warm and salty Atlantic water into the Arctic Ocean.

Forward particle trajectories reveal the fate of particles once they have passed the mooring site at 223 m depth (Fig. 4B). Particles were traced until they reached the seafloor. The average distance between the

particle positions at the seafloor and the mooring site in the experiments with sinking speeds of 53, 27 and 9 m d^{-1} is 50 km, 75 km and 141 km, respectively. Hence, in the experiment with the slow sinking velocity of 9 m d^{-1}, particles were exposed much more to the ocean currents in Fram Strait. Our study site is characterized by Atlantic Water carried with the West Spitsbergen Current, and the pattern in Fig. 4B visualises its pathway: One part of it recirculates in central Fram Strait and travels southwards with the East Greenland Current, another follows the western rim of the Yermak Plateau, and the remaining particles travel along the Svalbard shelf break into the Arctic Ocean.

3.4. Backtracking of sea ice as a potential vector for microplastics

The catchment areas determined by the Lagrangian particle tracking (Fig. 4A) are partly covered by sea ice. For catchment area I (underlying sinking velocity of particles: 53 m d^{-1}), for example, increased sea ice concentrations were recorded for autumn 2019, spring/summer 2020, and spring 2021. We backtracked sea ice to identify potential source regions, revealing the New Siberian Islands (between the Laptev Sea and East Siberian Sea) and the Laptev Sea (offshore) as sources of the sea ice present in the study area in autumn 2019 and spring/summer 2020, respectively (Fig. 5). For sea ice present in spring 2021, sea ice backtracking indicated the Kara Sea/Central Arctic Ocean as origins.

April 2021 showed strong intra-monthly variation with respect to sea ice origins: During the first week, sea ice appeared to originate from coastal areas in the western Laptev Sea (age: 3 years), and in mid/late April from the Nansen Basin (age: 1 year) (Fig. 6).
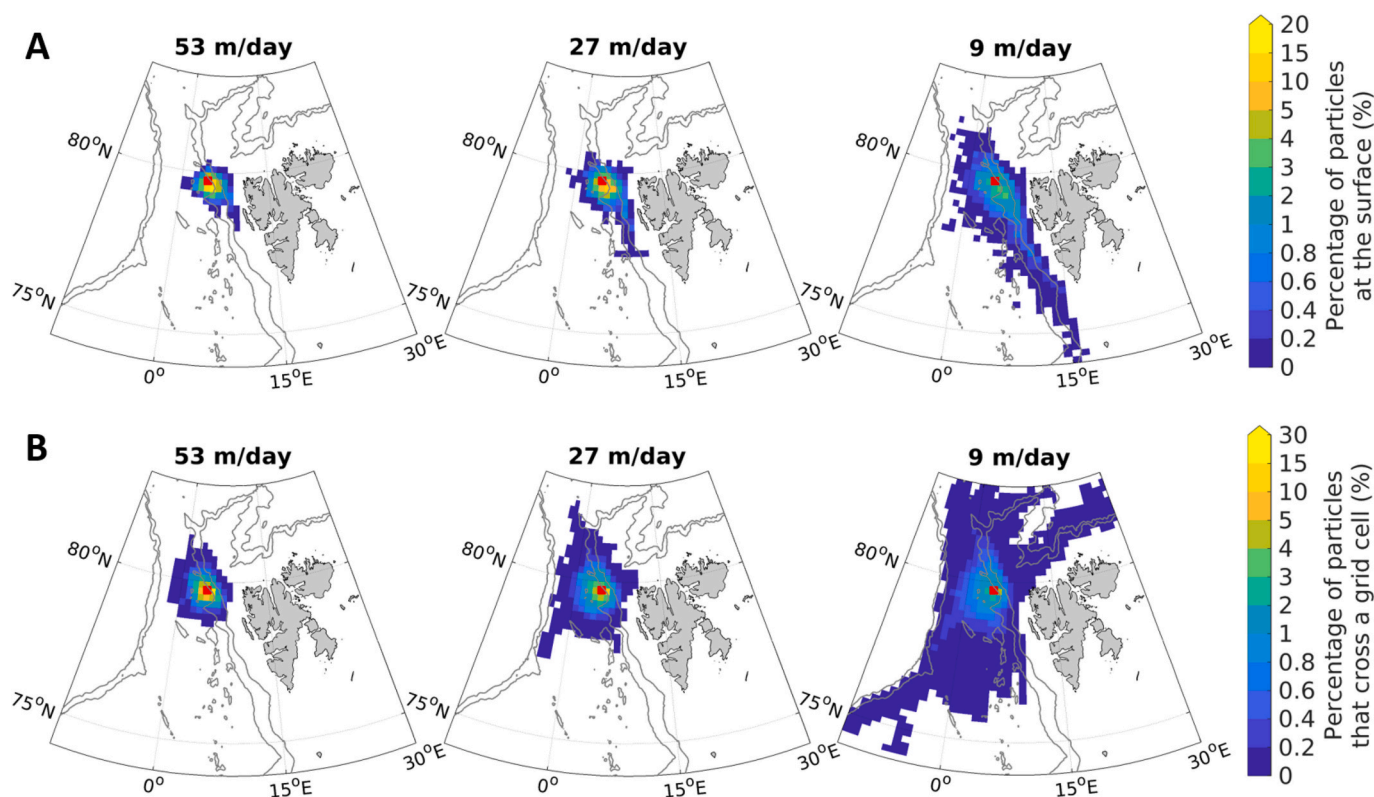

Fig. 4. Simulated backward and forward particle trajectories. (A) Catchment areas I-III (from left to right) of particles revealed from backward trajectories: Percentage of particles that reach the surface in a grid cell of size 1.0°longitude × 0.2°latitude. Trajectories were computed until the particles reached the sea surface. Three different sinking velocities were applied (53 m d^{-1}, 27 m d^{-1} and 9 m d^{-1}). (B) Fate of particles revealed from forward trajectories: Percentage of particles that cross a grid cell (1.0°longitude × 0.2°latitude) at least once. Trajectories were computed until the particles reached the seafloor. Three different sinking velocities were applied (53 m d^{-1}, 27 m d^{-1} and 9 m d^{-1}). The red square indicates the release location at HG-N4. Grey contours indicate the 1000 m and 2000 m isobaths.
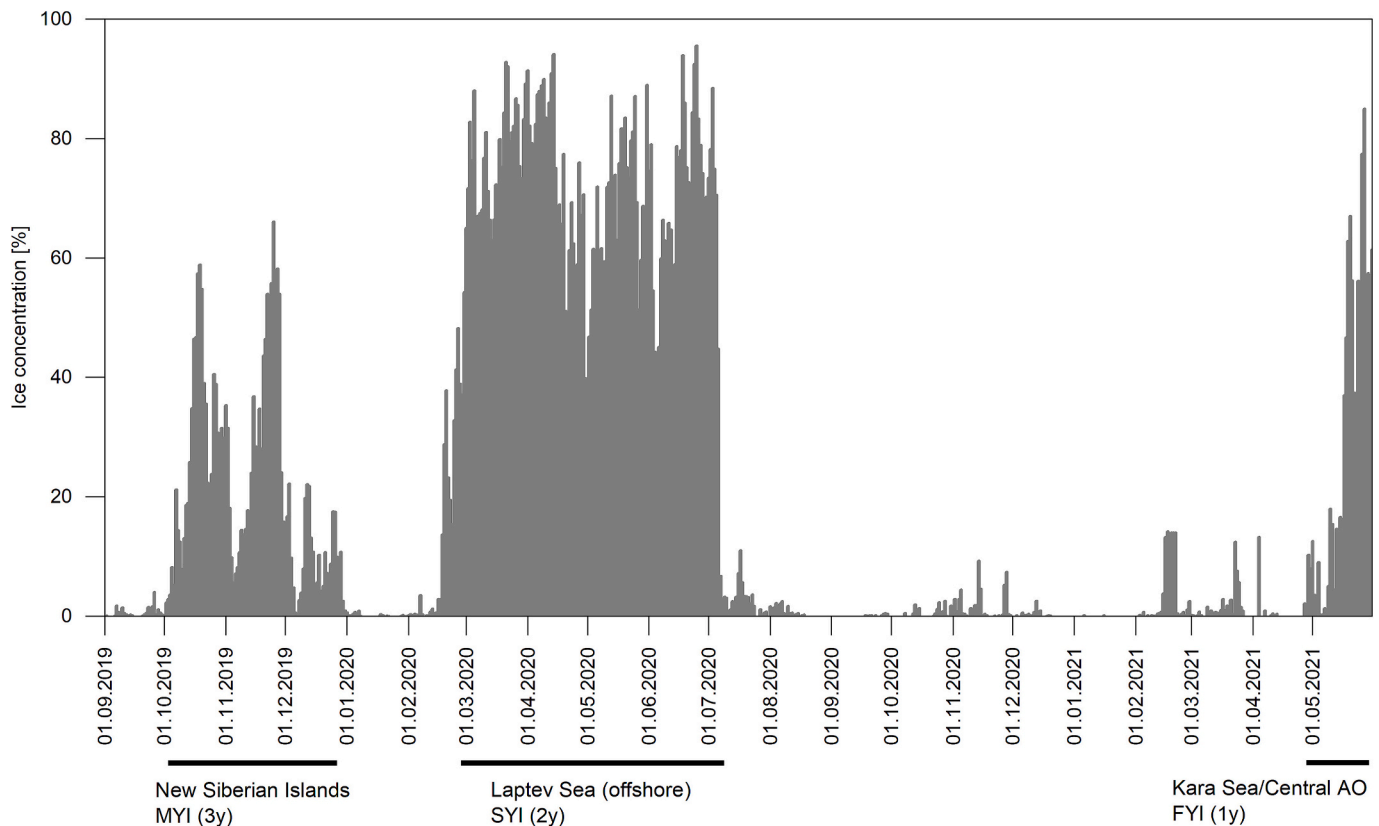
Fig. 5. Sea ice concentration and origin. Sea ice concentration for catchment area I (sinking velocity: 53 m d^{-1}) during the study period (September 2019 – May 2021). Potential origins were classified based on weekly backtracking of sea ice present in the catchment area. Abbreviations: FYI: first-year ice; SYI: second-year ice; MYI: multi-year ice.

4. Discussion

4.1. Inter-study comparison of microplastic pollution levels

This study assessed MP pollution patterns in the water column of Fram Strait, a key gateway between the Arctic Ocean and the Nordic seas, over a period of almost two years at high temporal resolution. Knowledge on seasonal MP fluxes in the ocean is scarce, especially with respect to longer periods, although the importance of MP time series data has been highlighted (Martin et al., 2023). In general, our recorded MP fluxes in the range of 0–2.9 MPs m^{-2} d^{-1} (Fig. 2A) are low compared to the fluxes recorded by Reineccius and Waniek (2022) for the sub-tropical Northeast Atlantic (1.1–3146.8 MPs m^{-2} d^{-1}). Sediment trap systems and minimum detection sizes (~10 μm) were comparable in both studies. Differences in sampling depths (2000 m vs. 230 m in our study) and site-specific hydrodynamic conditions could explain the differences in MP fluxes. The likelihood of observing rarer high-flux events could also be enhanced by the long observation period of twelve years. Higher values were also recorded by Rowlands et al. (2023) in an enclosed bay in the Southern Ocean, which could be due to high vessel activity. They detected decreasing MP fluxes from 50 m (306.3 MPs m^{-2} d^{-1}) to 150 m sampling depth (93.8 MPs m^{-2} d^{-1}) in a 24 h-deployment, suggesting higher particle fluxes near the sea surface. Similarly, Galgani et al. (2022) recorded plastics from 50 to 600 m depth in the North Atlantic Ocean, and nearly three quarters of the measured mass came from the upper 150 m. Given these sporadic observations and studies, we conclude that there are currently significant limitations of data availability and intercomparability, and we identify an urgent need for standardization and harmonization of sediment trap sampling approaches for the assessment of MP fluxes.

When considering MP studies in the Arctic, net, pump or bulk water

sampling by Niskin bottles and subsequent filtration were often used for water sampling (Lusher et al., 2015; Amélineau et al., 2016; Kanhai et al., 2018; Morgana et al., 2018; Tekman et al., 2020; Ikenoue et al., 2023), and multiple, gravity or piston corers for sediment sampling (Kanhai et al., 2019; Tekman et al., 2020). Our obtained MP data in the format of flux values (MPs m^{-2} d^{-1}) are therefore not directly comparable with respective concentration data in the units (MPs m^{-3}) or (MPs kg^{-1}). However, they provide an estimate for MP particle transport in the water column. Tekman et al. (2020) followed a holistic approach, looking at five sampling stations in Fram Strait, analysing water column samples from 2 to 4 different depths (0–1287 MPs m^{-3}) as well as sediment samples (239–13,331 MPs kg^{-1}). Within the water samples, which were collected using large-volume pumps, highest concentrations were always reported for samples from the near-surface layer (1–3 m). The relatively high MP levels recorded in these former studies for water and sediment appear to be in contrast with the present findings of comparatively low MP particle fluxes. Yet, it has to be kept in mind that no respective MP data exist yet for the station described here (HG-N4) in the HAUSGARTEN observatory. Hence, other locations in that area may show differing MP fluxes. Furthermore, it should be noted that MP particles do not necessarily reach greater water depths as individual particles or small aggregates, but can also be transported downwards in larger aggregates (such as clumps of the ice algae *Melosira arctica*). These cannot be adequately captured by sediment traps or could bypass them, possibly leading to an underestimation of MP abundances in some samples. Overall, more research is needed to gain insights into flux patterns within the Arctic with a higher spatial resolution, allowing for a comprehensive comparison between different locations and better understand vertical transport of MPs.

Concerning size distributions, the highest MP abundances were recorded in the smallest size classes (Fig. 3B), which concurs with
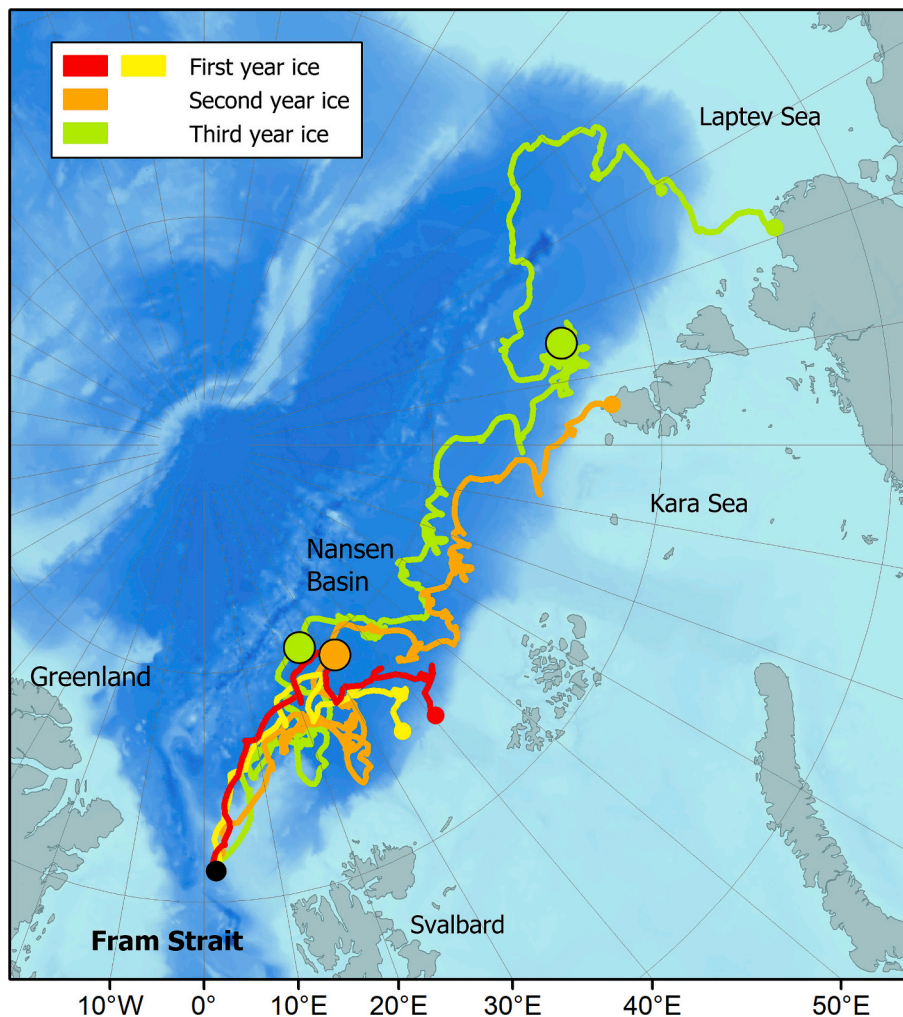
Fig. 6. Trajectories and origin of sea ice. Displayed are the results of sea ice backtracking on a weekly basis (green: 01–07 April 2021; orange: 08–14 April 2021; yellow: 15–21 April 2021; red: 22–28 April2021). Dots with black outlines indicate the transition from one age class to the next one.

previous studies (Bergmann et al., 2017; Tekman et al., 2020) and is likely to be more problematic in terms of uptake by organisms. Indeed, zooplankton samples from ten stations in Fram Strait showed that all five analysed species and most specimens had ingested MPs (Botterell et al., 2022). Overall, the ubiquity of MPs in all compartments in Fram Strait is a concern given its remoteness, and requires further attention to assess and, most importantly, reduce plastic pollution.

For the assessment of MP abundances, we applied ATR-FTIR and μ-FTIR for different size fractions, as performed in previous studies on MP in Arctic environments (Bergmann et al., 2017; Peeken et al., 2018; Bergmann et al., 2019; Tekman et al., 2020).This approach provides data on the number of MPs, while the complementary assessment of mass data is recommended wherever possible (Primpke et al., 2022). In line with the ongoing efforts to harmonize methodological approaches, we additionally present the obtained data for both MP size fractions in the reporting format proposed by Primpke et al. (2022) with respect to polymer types and size categories (Appendix C). Shape and colour types suggested in Primpke et al. (2022), however, were only assigned to the respective categories for the >500 μm sample fraction. This is due to the fact that the semi-automated μ-FTIR imaging method used for S-MP (<500 μm) does not provide information on particle morphology at this level of detail, and a visual assessment of small items <300 μm is challenging. Finally, further efforts regarding standardization of sampling, analytical techniques and data reporting are required, and highly recommended for future assessments, in order to move towards a better

comparability of MP data.

4.2. Temporal patterns of microplastic fluxes in Fram Strait, Arctic and potential drivers

The high temporal resolution of the sampling allowed for a comprehensive insight into the MP fluxes over time. Our data show increased seasonal MP fluxes in both April 2020 and 2021, suggesting an influence of the underlying biogeochemical and physical parameters (Fig. 2). Their analysis could partly explain the variability in MP fluxes, but also underscores their high complexity. The increased MP flux in April 2020 coincides with a slight increase in seston, especially POM (Fig. 2B). In April 2021, this relationship was even more pronounced. Furthermore, a weak positive correlation was found for MP and biogenic flux (Appendix A, Table A1). These observations indicate a potential entrapment of MPs in aggregates of biogenic origin, acting as a transport vector for MPs. Accordingly, a positive correlation between MP in the water column and particulate matter was observed in Tekman et al. (2020), as well as between MPs and chlorophyll *a* content in sediments in Fram Strait (Bergmann et al., 2017) implying vertical export via incorporation in sinking algal aggregates. In laboratory experiments, biological aggregates were shown to entrain and transport MPs (Michels et al., 2018; Wang et al., 2021b). Increased dinosterol fluxes in April 2021 and especially in April 2020 further suggest a possible interaction with dinoflagellate phytoplankton, although this hypothesis needs

validation. Concerning temporal patterns of polymer types, CPE was present in October 2019 and re-occurred in October 2020. In addition, polymer compositions in April 2020 and 2021 were similar. In contrast, the occurrence of PS was limited to the period from November 2019 to March 2020. Size class distributions were dominated by particles <25 μm throughout the study period, with larger particles (>100 μm) only detected in March, April, and October 2020. These patterns should, however, be interpreted with caution, as particle counts were generally <10, limiting the representativeness with respect to polymer compositions.

Beside the above-mentioned biogeochemical variables, also physical variables may influence temporal patterns of MP fluxes. For example, in April 2021 the current direction was mainly south-eastwards (Fig. A1), indicating an increased transport of material from the East Greenland shelf. Moreover, previous studies showed that Arctic sea ice entrains MPs, suggesting potential long-distance transport during ice drift and release to the water column during melting (Peeken et al., 2018; Kanhai et al., 2020; Kim et al., 2021). Accordingly, MP abundances in benthic organisms from the Chukchi Sea were positively correlated with reduced sea ice coverage and hence sea ice melting (Fang et al., 2021). The first MP peak in April 2020 coincides with a period of dwindling sea ice, suggesting a potential impact by vertically transported ice-derived matter. In this context, ice-related organisms could play an important role in vertical transport mechanisms: For example, the ice-associated algae *Melosira arctica* was shown to entrain high quantities of MPs in their filaments, and likely acts as a transport vehicle from the ocean surface to the deep seafloor (Boetius et al., 2013; Bergmann et al., 2023). We did not observe *Melosira arctica* in the samples, however, it has to be noted that sediment traps may not adequately capture them due to the formation of large aggregates that may fall past the traps. Concerning the here analysed biomarker IP_{25}, indicating the presence of other sea-ice associated diatoms (Belt et al., 2007; Brown et al., 2014), no correlation with MPs was found in our study (Fig. 2, Table A1).

In summary, the present study shows that total MP fluxes in FRAM Strait vary over near-monthly time scales, with maxima in April 2020 and April 2021. As stated above, these high flux events coincided with the underlying biogeochemical and physical variables to different extents, however, a clear identification of drivers was not possible in the framework of this study and will need further investigation. Although polymer compositions and size class distributions showed a certain variation over time as well (Fig. 3A+B), the low counts of individual polymer types or size classes hamper deeper interpretation. Nevertheless, the MP flux data presented here represent, to our knowledge, the first time series at this location in Fram Strait, Arctic, and attempt to contribute to a better understanding of MP pollution in this region.

4.3. Potential sources and pathways of microplastics

In addition to environmental MP data, this study included particle and sea ice modelling to predict possible past and future transport routes of MPs. For the prediction of particle trajectories, a FESOM model was applied (cf. Section 2.6). In addition to backward simulations, which had been computed in a similar way in Tekman et al. (2020), we also determined forward simulations of particle trajectories, predicting the location where particles would reach the seafloor. In both types of simulations, it was obvious that a low sinking velocity leads to increased catchment and settling areas, respectively (Section 3.3, Fig. 4). This is especially due to a higher impact of ocean currents on particles in this scenario, as described in previous works (Wekerle et al., 2018; Tekman et al., 2020). The forward simulations based on low sinking velocities, e. g. predicted an average travel distance of 141 km (compared to 75 km and 50 km calculated for the higher sinking velocities) between the release location HG-N4 and the end position on the seafloor (Fig. 4B). The strong variability of resulting catchment and settling areas in relation to the different sinking velocity scenarios emphasizes the complex nature of particle transport behavior, also in light of the high variety of

MP types (e.g., regarding polymers and shapes) and respective aggregation behavior.

In the context of long-distance transportation of MPs, this study also investigated sea ice as potential transport vector. Herein, backtracking of sea ice for spring 2020 revealed that sea ice present in the modelled catchment area I originated primarily from the Laptev Sea, whereas autumn 2019 and spring 2021 showed other potential origins (New Siberian Islands and Kara Sea/central Atlantic Ocean, respectively) (Section 3.4, Fig. 5). For catchment areas II and III, sea ice origins are expected to be similar: The underlying lower sinking velocities of these catchments lead to an expansion in a north-south direction (Section 3.3, Fig. 4) (Wekerle et al., 2018), whereas the ice regime in Fram Strait mainly follows an east-west gradient (Krumpen et al., 2019) and is therefore not expected to be strongly impacted by differences in catchment areas.

Backtracking of sea ice on a weekly basis revealed that April 2021 differed from all other sampling months, showing intra-monthly variations: For the first week of this month, the coastal area of the western Laptev Sea was identified as a potential ice source (Fig. 6). Nearby, the Chatanga River discharges and could transport MPs to the Laptev Sea. Initial evidence from the rivers and/or estuaries of the Ob, Tom, Yenisei and Lena showed the presence of MP in the water (Frank et al., 2021; Yakushev et al., 2021) and fish (Frank et al., 2023) of Siberian rivers. Furthermore, for the second half of April 2021, the modelled sea ice origin was located closer to the mooring, in the Nansen Basin (Fig. 6). In a study of near-surface water samples collected from the East Asian Seas to the Central Arctic Basin, the Nansen Basin was characterized by the highest concentrations (Huang et al., 2022). Accordingly, this area was projected to be an accumulation zone for MPs (Huserbråten et al., 2022). These results suggest that MPs could be entrained during ice formation in the Nansen Basin, and is subsequently transported to Fram Strait. Although the sea ice backtracking provides an insight into possible source regions, the actual magnitude of the contribution to local MP fluxes requires further investigation.

The particle and sea ice modelling applied here provided insights into potential sources and pathways of MPs present at the HG-N4 station in Fram Strait. Different particle transport scenarios were suggested, with simulated particle trajectories being highly influenced by the applied sinking velocities. Sea ice modelling revealed varying potential source regions for different periods, with sea ice partly originating from coastal areas with riverine input, which may be of interest with respect to MP inclusion and subsequent transport. It has to be noted that particle and sea-ice modelling represent a simplification of the highly complex natural conditions prevalent in the Arctic. Nevertheless, we believe it is important to attempt source tracking to better understand potential MP pathways and to get an idea of which locations may be relevant for future assessments. More research is needed in order to elucidate these processes further and thereby better understand potential origins and distribution patterns of MPs in the Arctic.

5. Conclusion

This study provides an unprecedented high-resolution dataset of MP pollution in Fram Strait based on sediment trap samples, spanning a period of almost two years, and investigates potential drivers of MP flux variability. Contextualization in terms of underlying biogeochemical and physical parameters showed a high level of complexity: a temporal trend was evident, with both MP flux maxima in April 2020 and April 2021 showing similar magnitudes and polymer compositions. However, they appear to be influenced to different extents by factors such as seston, sea ice concentration, sea ice origin characteristics, and ocean current conditions. This rather complex interplay of different parameters requires further investigation to gain additional insight into the MP flux dynamics in Arctic waters. Interestingly, all detected MP particles were <300 μm in size, highlighting the importance of including these size fractions in MP assessments. Furthermore, in order to better

compare sediment trap studies on a global scale, we strongly suggest a harmonized analytical protocol (sediment trap type, polymer typology used, sample processing and analytical methods), possibly in the form of a consistent, parallel international monitoring effort, also taking into account seasonality and potential environmental drivers. Finally, particle tracking models and sea ice backtracking, as performed in this study, can contribute to a better understanding of potential MP sources and distribution patterns.

CRediT authorship contribution statement

Lisa Roscher: Writing – review & editing, Writing – original draft, Visualization, Investigation, Data curation. **Eva-Maria Nöthig:** Conceptualization, Writing – review & editing. **Kirsten Fahl:** Methodology, Writing – review & editing. **Claudia Wekerle:** Methodology, Visualization, Writing – review & editing. **Thomas Krumpen:** Methodology, Visualization, Writing – review & editing. **Mario Hoppmann:** Methodology, Writing – review & editing. **Nadine Knüppel:** Investigation, Writing – review & editing. **Sebastian Primpke:** Data curation, Software, Validation, Writing – review & editing. **Gunnar Gerdts:** Writing – review & editing. **Melanie Bergmann:** Conceptualization, Supervision, Writing – review & editing.

Declaration of competing interest

The authors declare that they have no known competing financial interests or personal relationships that could have appeared to influence the work reported in this paper.

Appendix A. Supplementary data

Supplementary data to this article can be found online at https://doi.org/10.1016/j.scitotenv.2024.178035.

Data availability

Mooring raw data is available under https://doi.pangaea.de/10.1594/PANGAEA.946533.

References

Abel, S.M., Primpke, S., Int-Veen, I., Brandt, A., Gerdts, G., 2021. Systematic identification of microplastics in abyssal and hadal sediments of the Kuril Kamchatka trench. Environ. Pollut. 269, 116095. https://doi.org/10.1016/j.envpol.2020.116095.

Abel, S.M., Primpke, S., Wu, F., Brandt, A., Gerdts, G., 2022. Human footprints at hadal depths: interlayer and intralayer comparison of sediment cores from the Kuril Kamchatka trench. Sci. Total Environ. 838, 156035. https://doi.org/10.1016/j.scitotenv.2022.156035.

Alfred-Wegener-Institut Helmholtz-Zentrum für Polar- und Meeresforschung, 2023. Marine Stations Helgoland and Sylt operated by the Alfred Wegener Institute Helmholtz Centre for Polar and Marine Research. J. Large-Scale Res. Facil. 8, A184. https://doi.org/10.17815/jlsrf-8-184.

Allen, S., Allen, D., Karbalaei, S., Maselli, V., Walker, T.R., 2022. Micro(nano)plastics sources, fate, and effects: what we know after ten years of research. Journal of Hazardous Materials Advances 6, 100057. https://doi.org/10.1016/j.hazadv.2022.100057.

AMAP, 2021. AMAP Litter and Microplastics Monitoring Guidelines. Version 1.0. Arctic Monitoring and Assessment Programme. https://doi.org/10.25607/OBP-1667.

Amélineau, F., Bonnet, D., Heitz, O., Mortreux, V., Harding, A.M., Karnovsky, N., Walkusz, W., Fort, J., Grémillet, D., 2016. Microplastic pollution in the Greenland Sea: background levels and selective contamination of planktivorous diving seabirds. Environ. Pollut. 219, 1131–1139. https://doi.org/10.1016/j.envpol.2016.09.017.

Belt, S., Massé, G., Rowland, S., Poulin, M., Michel, C., Leblanc, B., 2007. A novel chemical fossil of palaeo sea ice: IP25. Org. Geochem. 38, 16–27. https://doi.org/10.1016/j.orggeochem.2006.09.013.

Bergmann, M., Wirzberger, V., Krumpen, T., Lorenz, C., Primpke, S., Tekman, M.B., Gerdts, G., 2017. High quantities of microplastic in Arctic Deep-Sea sediments from the HAUSGARTEN observatory. Environ. Sci. Technol. 51, 11000–11010. https://doi.org/10.1021/acs.est.7b03331.

Bergmann, M., Mützel, S., Primpke, S., Tekman, M.B., Trachsel, J., Gerdts, G., 2019. White and wonderful? Microplastics prevail in snow from the Alps to the Arctic. Sci. Adv. 5. https://doi.org/10.1126/sciadv.aax1157 eaax1157.

Bergmann, M., Collard, F., Fabres, J., Gabrielsen, G.W., Provencher, J.F., Rochman, C.M., van Sebille, E., Tekman, M.B., 2022. Plastic pollution in the Arctic. Nature Reviews Earth & Environment 3, 323–337.

Bergmann, M., Allen, S., Krumpen, T., Allen, D., 2023. High levels of microplastics in the Arctic Sea ice alga Melosira arctica, a vector to ice-associated and benthic food webs. Environ. Sci. Technol. 57, 6799–6807. https://doi.org/10.1021/acs.est.2c08010.

Bodungen, B.V., Wunsch, M., Fürderer, H., 1991. Sampling and Analysis of Suspended and Sinking Particles in the Northern North Atlantic. Seiten 47–56 Marine Particles: Analysis and Characterization. https://doi.org/10.1029/GM063p0047.

Boetius, A., Albrecht, S., Bakker, K., Bienhold, C., Felden, J., Fernández-Méndez, M., Hendricks, S., Katlein, C., Lalande, C., Krumpen, T., Nicolaus, M., Peeken, I., Rabe, B., Rogacheva, A., Rybakova, E., Somavilla, R., Wenzhöfer, F., Party, R.P.A.-.-S.S., 2013. Export of algal biomass from the melting Arctic Sea ice. Science 339, 1430–1432. https://doi.org/10.1126/science.1231346.

Boon, J.J., Rijpstra, W.I.C., de Lange, F., De Leeuw, J., Yoshioka, M., Shimizu, Y., 1979. Black Sea sterol—a molecular fossil for dinoflagellate blooms. Nature 277, 125–127. https://doi.org/10.1038/277125a0.

Botterell, Z.L.R., Bergmann, M., Hildebrandt, N., Krumpen, T., Steinke, M., Thompson, R. C., Lindeque, P.K., 2022. Microplastic ingestion in zooplankton from the Fram Strait in the Arctic. Sci. Total Environ. 831, 154886. https://doi.org/10.1016/j.scitotenv.2022.154886.

Brown, T.A., Belt, S.T., Tatarek, A., Mundy, C.J., 2014. Source identification of the Arctic sea ice proxy IP25. Nat. Commun. 5, 4197. https://doi.org/10.1038/ncomms5197.

Clarke, K., Gorley, R., 2015. PRIMER version 7: user manual/tutorial. PRIMER-E 192.

Collard, F., Ask, A., 2021. Plastic ingestion by Arctic fauna: a review. Sci. Total Environ. 786, 147462. https://doi.org/10.1016/j.scitotenv.2021.147462.

Dee, D.P., Uppala, S.M., Simmons, A.J., Berrisford, P., Poli, P., Kobayashi, S., Andrae, U., Balmaseda, M., Balsamo, G., Bauer, d.P., 2011. The ERA-interim reanalysis: configuration and performance of the data assimilation system. Q. J. R. Meteorol. Soc. 137, 553–597. https://doi.org/10.1002/qj.828.

Ezraty, R., Girard-Ardhuin, F., Piolle, J.-f., Kaleschke, L., Heygster, G., 2007. Arctic & Antarctic Sea Ice Concentration and Arctic Sea Ice Drift Estimated From Special Sensor MIcrowave Data - User's Manual V2.1.

Fahl, K., Stein, R., 2012. Modern seasonal variability and deglacial/Holocene change of central Arctic Ocean sea-ice cover: new insights from biomarker proxy records. Earth Planet. Sci. Lett. 351, 123–133. https://doi.org/10.1016/j.epsl.2012.07.009.

Fang, C., Zheng, R., Hong, F., Jiang, Y., Chen, J., Lin, H., Lin, L., Lei, R., Bailey, C., Bo, J., 2021. Microplastics in three typical benthic species from the Arctic: occurrence, characteristics, sources, and environmental implications. Environ. Res. 192, 110326. https://doi.org/10.1016/j.envres.2020.110326.

Frank, Y., Vorobiev, D., Mandal, A., Lemeshko, Y., Rakhmatullina, S., Darbha, G.K., 2023. Freshwater fish Siberian dace ingest microplastics in the remote Yenisei Tributary. Toxics 11, 38. https://doi.org/10.3390/toxics11010038.

Frank, Y.A., Vorobiev, E.D., Vorobiev, D.S., Trifonov, A.A., Antsiferov, D.V., Soliman Hunter, T., Wilson, S.P., Strezov, V., 2021. Preliminary screening for microplastic concentrations in the surface water of the Ob and Tom Rivers in Siberia, Russia. Sustainability 13, 80. https://doi.org/10.3390/su13010080.

Galgani, L., Goßmann, I., Scholz-Böttcher, B., Jiang, X., Liu, Z., Scheidemann, L., Schlundt, C., Engel, A., 2022. Hitchhiking into the deep: how microplastic particles are exported through the biological carbon pump in the North Atlantic Ocean. Environ. Sci. Technol. 56, 15638–15649. https://doi.org/10.1021/acs.est.2c04712.

Hoppmann, M., von Appen, W.-J., Bienhold, C., Frommhold, L., Hagemann, J., Hargesheimer, T., Iversen, M.H., Knüppel, N., Konrad, C., Lochthofen, N., Ludszuweit, J., Monsees, M., McPherson, R., Nicolaus, A., Nöthig, E.-M., Metfies, K., Soltwedel, T., 2022. Raw physical oceanography, ocean current velocity and particle export data from mooring HG-N-FEVI-39 in the Fram Strait, September 2019–June 2021. In: Hoppmann, Mario (Ed.), Collection of Raw Data From Oceanographic Moorings in the Fram Strait, Greenland Sea, and central Arctic Ocean, 2018–2025. PANGAEA. https://doi.pangaea.de/10.1594/PANGAEA.959812 (dataset in review). PANGAEA.

Huang, W.-Y., Meinschein, W.G., 1979. Sterols as ecological indicators. Geochim. Cosmochim. Acta 43, 739–745. https://doi.org/10.1016/0016-7037(79)90257-6.

Huang, Y., Zhang, W., Zhang, S., Jin, F., Fang, C., Ma, X., Wang, J., Mu, J., 2022. Systematical insights into distribution and characteristics of microplastics in near-surface waters from the East Asian Seas to the Arctic Central Basin. Sci. Total Environ. 814, 151923. https://doi.org/10.1016/j.scitotenv.2021.151923.

Huserbråten, M.B.O., Hattermann, T., Broms, C., Albretsen, J., 2022. Trans-polar drift-pathways of riverine European microplastic. Sci. Rep. 12, 3016. https://doi.org/10.1038/s41598-022-07080-z.

Ikenoue, T., Nakajima, R., Mishra, P., Ramasamy, E.V., Fujiwara, A., Nishino, S., Murata, A., Watanabe, E., Itoh, M., 2023. Floating microplastic inventories in the southern Beaufort Sea, Arctic Ocean. Front. Mar. Sci. 10. https://doi.org/10.3389/fmars.2023.1288301.

Kanhai, L.D.K., Gårdfeldt, K., Lyashevska, O., Hassellöv, M., Thompson, R.C., O'Connor, I., 2018. Microplastics in sub-surface waters of the Arctic Central Basin. Mar. Pollut. Bull. 130, 8–18. https://doi.org/10.1016/j.marpolbul.2018.03.011.

Kanhai, L.D.K., Johansson, C., Frias, J.P.G.L., Gardfeldt, K., Thompson, R.C., O'Connor, I., 2019. Deep sea sediments of the Arctic Central Basin: a potential sink for microplastics. Deep-Sea Res. I Oceanogr. Res. Pap. 145, 137–142. https://doi.org/10.1016/j.dsr.2019.03.003.

Kanhai, L.D.K., Gardfeldt, K., Krumpen, T., Thompson, R.C., O'Connor, I., 2020. Microplastics in sea ice and seawater beneath ice floes from the Arctic Ocean. Sci. Rep. 10, 5004. https://doi.org/10.1038/s41598-020-61948-6.

Kim, S.-K., Lee, H.-J., Kim, J.-S., Kang, S.-H., Yang, E.-J., Cho, K.-H., Tian, Z., Andrady, A., 2021. Importance of seasonal sea ice in the western Arctic ocean to the Arctic and global microplastic budgets. J. Hazard. Mater. 418, 125971. https://doi.org/10.1016/j.jhazmat.2021.125971.

Krumpen, T., Belter, H.J., Boetius, A., Damm, E., Haas, C., Hendricks, S., Nicolaus, M., Nöthig, E.-M., Paul, S., Peeken, I., Ricker, R., Stein, R., 2019. Arctic warming interrupts the transpolar drift and affects long-range transport of sea ice and ice-rafted matter. Sci. Rep. 9, 5459. https://doi.org/10.1038/s41598-019-41456-y.

Krumpen, T., Birrien, F., Kauker, F., Rackow, T., von Albedyll, L., Angelopoulos, M., Belter, H.J., Bessonov, V., Damm, E., Dethloff, K., Haapala, J., Haas, C., Harris, C., Hendricks, S., Hoelemann, J., Hoppmann, M., Kaleschke, L., Karcher, M., Kolabutin, N., Lei, R., Lenz, J., Morgenstern, A., Nicolaus, M., Nixdorf, U., Petrovsky, T., Rabe, B., Rabenstein, L., Rex, M., Ricker, R., Rohde, J., Shimanchuk, E., Singha, S., Smolyanitsky, V., Sokolov, V., Stanton, T., Timofeeva, A., Tsamados, M., Watkins, D., 2020. The MOSAiC ice floe: sediment-laden survivor from the Siberian shelf. Cryosphere 14, 2173–2187. https://doi.org/10.5194/tc-14-2173-2020.

Lavergne, T., 2016. Validation and Monitoring of the OSI SAF Low Resolution Sea Ice Drift Product (v5).

Löder, M., Imhof, H., Ladehoff, M., Löschel, L., Lorenz, C., Mintenig, S., Piehl, S., Primpke, S., Schrank, I., Laforsch, C., Gerdts, G., 2017. Enzymatic purification of microplastics in environmental samples. Environ. Sci. Technol. 51, 14283–14292. https://doi.org/10.1021/acs.est.7b03055.

Lusher, A.L., Bråte, I.L., Munno, K., Hurley, R., Welden, N., 2020. EXPRESS: is it or Isn't it: the importance of visual classification in microplastic characterization. Appl. Spectrosc. 74, 1139–1153. https://doi.org/10.1177/0003702820930733.

Lusher, A.L., Tirelli, V., O'Connor, I., Officer, R., 2015. Microplastics in Arctic polar waters: the first reported values of particles in surface and sub-surface samples. Sci. Rep. 5, 14947. https://doi.org/10.1038/srep14947.

Martin, J., Granberg, M., Provencher, J.F., Liborion, M., Pijogge, L., Magnusson, K., Hallanger, I.G., Bergmann, M., Aliani, S., Gomiero, A., Grøsvik, B.E., Vermaire, J., Primpke, S., Lusher, A.L., 2023. The power of multi-matrix monitoring in the Pan-Arctic region: plastics in water and sediment. Arctic Science 9, 146–164. https://doi.org/10.1139/as-2021-0056.

Metfies, K., 2020. The expedition PS121 of the research vessel POLARSTERN to the Fram Strait in 2019. Berichte zur Polar-und Meeresforschung= Reports on polar and marine research 738. https://doi.org/10.2312/BzPM_0738_2020.

Michels, J., Stippkugel, A., Lenz, M., Wirtz, K., Engel, A., 2018. Rapid aggregation of biofilm-covered microplastics with marine biogenic particles. Proc. R. Soc. B 285, 20181203. https://doi.org/10.1098/rspb.2018.1203.

Miller, M.E., Hamann, M., Kroon, F.J., 2020. Bioaccumulation and biomagnification of microplastics in marine organisms: a review and meta-analysis of current data. PLoS One 15, e0240792. https://doi.org/10.1371/journal.pone.0240792.

Morgana, S., Ghigliotti, L., Estévez-Calvar, N., Stifanese, R., Wieckzorek, A., Doyle, T., Christiansen, J.S., Faimali, M., Garaventa, F., 2018. Microplastics in the Arctic: a case study with sub-surface water and fish samples off Northeast Greenland. Environ. Pollut. 242, 1078–1086. https://doi.org/10.1016/j.envpol.2018.08.001.

Norén, F., 2007. Small Plastic Particles in Coastal Swedish Waters. KIMO Sweden, N-Research, Lysekil, Sweden.

Obbard, R., Sadri, S., Wong, Y.-Q., Khitun, A., Baker, I., Thompson, R., 2014. Global warming releases microplastic legacy frozen in Arctic Sea ice. Earth's Future 2, 315–320. https://doi.org/10.1002/2014EF000240.

Ostle, C., Thompson, R.C., Broughton, D., Gregory, L., Wootton, M., Johns, D.G., 2019. The rise in ocean plastics evidenced from a 60-year time series. Nat. Commun. 10, 1622. https://doi.org/10.1038/s41467-019-09506-1.

Parga Martínez, K.B., Tekman, M.B., Bergmann, M., 2020. Temporal trends in marine litter at three stations of the HAUSGARTEN Observatory in the Arctic Deep sea. Front. Mar. Sci. 7, 321. https://doi.org/10.3389/fmars.2020.00321.

Peeken, I., Primpke, S., Beyer, B., Gütermann, J., Katlein, C., Krumpen, T., Bergmann, M., Hehemann, L., Gerdts, G., 2018. Arctic sea ice is an important temporal sink and means of transport for microplastic. Nat. Commun. 9, 1505. https://doi.org/10.1038/s41467-018-03825-5.

Poon, F.E., Provencher, J.F., Mallory, M.L., Braune, B.M., Smith, P.A., 2017. Levels of ingested debris vary across species in Canadian Arctic seabirds. Mar. Pollut. Bull. 116 (1–2), 517–520. https://doi.org/10.1016/j.marpolbul.2016.11.051.

Primpke, S., Lorenz, C., Rascher-Friesenhausen, R., Gerdts, G., 2017. An automated approach for microplastics analysis using focal plane array (FPA) FTIR microscopy and image analysis. Anal. Methods 9, 1499–1511. https://doi.org/10.1039/C6AY02476A.

Primpke, S., Dias, P., Gerdts, G., 2019. Automated identification and quantification of microfibres and microplastics. Anal. Methods 11, 2138–2147. https://doi.org/10.1039/C9AY00126C.

Primpke, S., Cross, R.K., Mintenig, S.M., Simon, M., Vianello, A., Gerdts, G., Vollertsen, J., 2020. Toward the systematic identification of microplastics in the environment: evaluation of a new independent software tool (siMPle) for spectroscopic analysis. Appl. Spectrosc. 74, 1127–1138. https://doi.org/10.1177/0003702820917760.

Primpke, S., Booth, A.M., Gerdts, G., Gomiero, A., Kögel, T., Lusher, A.L., Strand, J., Scholz-Böttcher, B.M., Galgani, F., Provencher, J.F., Aliani, S., Patankar, S., Vorkamp, K., 2022. Monitoring of microplastic pollution in the Arctic: recent developments in polymer identification, quality assurance and control (QA/QC), and data reporting. Arctic Science 9 (1), 176–197. https://doi.org/10.1139/as-2022-0006.

Reineccius, J., Waniek, J.J., 2022. First long-term evidence of microplastic pollution in the deep subtropical Northeast Atlantic. Environ. Pollut. 305, 119302. https://doi.org/10.1016/j.envpol.2022.119302.

Roscher, L., Fehres, A., Reisel, L., Halbach, M., Scholz-Böttcher, B., Gerriets, M., Badewien, T.H., Shiravani, G., Wurpts, A., Primpke, S., Gerdts, G., 2021. Microplastic pollution in the Weser estuary and the German North Sea. Environ. Pollut. 288, 117681. https://doi.org/10.1016/j.envpol.2021.117681.

Roscher, L., Halbach, M., Nguyen, M.T., Hebeler, M., Luschtinez, F., Scholz-Böttcher, B. M., Primpke, S., Gerdts, G., 2022. Microplastics in two German wastewater treatment plants: year-long effluent analysis with FTIR and Py-GC/MS. Sci. Total Environ. 817, 152619. https://doi.org/10.1016/j.scitotenv.2021.152619.

Rosso, B., Scoto, F., Hallanger, I.G., Larose, C., Gallet, J.C., Spolaor, A., Bravo, B., Barbante, C., Gambaro, A., Corami, F., 2024. Characteristics and quantification of small microplastics (<100 μm) in seasonal svalbard snow on glaciers and lands. J. Hazard. Mater. 467, 133723. https://doi.org/10.1016/j.jhazmat.2024.133723.

Rowlands, E., Galloway, T., Cole, M., Peck, V.L., Posacka, A., Thorpe, S., Manno, C., 2023. Vertical flux of microplastic, a case study in the Southern Ocean, South Georgia. Mar. Pollut. Bull. 193, 115117. https://doi.org/10.1016/j.marpolbul.2023.115117.

Schlitzer, R., 2022. Ocean Data View. https://odv.awi.de.

Soltwedel, T., 2021. The expedition PS126 of the research vessel POLARSTERN to the Fram Strait in 2021. Berichte zur Polar-und Meeresforschung= Reports on polar and marine research 757. https://doi.org/10.48433/BzPM_0757_2021.

Soltwedel, T., Bauerfeind, E., Bergmann, M., Bracher, A., Budaeva, N., Busch, K., Cherkasheva, A., Fahl, K., Grzelak, K., Hasemann, C., Jacob, M., Kraft, A., Lalande, C., Metfies, K., Nöthig, E.-M., Meyer, K., Quéric, N.-V., Schewe, I., Włodarska-Kowalczuk, M., Klages, M., 2016. Natural variability or anthropogenically-induced variation? Insights from 15 years of multidisciplinary observations at the arctic marine LTER site HAUSGARTEN. Ecol. Indic. 65, 89–102. https://doi.org/10.1016/j.ecolind.2015.10.001.

Tekman, M.B., Wekerle, C., Lorenz, C., Primpke, S., Hasemann, C., Gerdts, G., Bergmann, M., 2020. Tying up loose ends of microplastic pollution in the Arctic: distribution from the sea surface through the water column to Deep-Sea sediments at the HAUSGARTEN observatory. Environ. Sci. Technol. 54, 4079–4090. https://doi.org/10.1021/acs.est.9b06981.

Tekman, M.B., Walther, B., Peter, C., Gutow, L., Bergmann, M., 2022. Impacts of plastic pollution in the oceans on marine species, biodiversity and ecosystems. WWW Germany. https://doi.org/10.5281/zenodo.5898684.

Vitali, C., Peters, R.J.B., Janssen, H.-G., Undas, A.K., Munniks, S., Ruggeri, F.S., Nielen, M.W.F., 2024. Quantitative image analysis of microplastics in bottled water using artificial intelligence. Talanta 266, 124965. https://doi.org/10.1016/j.talanta.2023.124965.

Volkman, J.K., 1986. A review of sterol markers for marine and terrigenous organic matter. Org. Geochem. 9, 83–99. https://doi.org/10.1016/0146-6380(86)90089-6.

Wang, F., Wu, H., Wu, W., Wang, L., Liu, J., An, L., Xu, Q., 2021a. Microplastic characteristics in organisms of different trophic levels from Liaohe Estuary, China. Sci. Total Environ. 789, 148027. https://doi.org/10.1016/j.scitotenv.2021.148027.

Wang, X., Bolan, N., Tsang, D.C., Sarkar, B., Bradney, L., Li, Y., 2021b. A review of microplastics aggregation in aquatic environment: influence factors, analytical methods, and environmental implications. J. Hazard. Mater. 402, 123496. https://doi.org/10.1016/j.jhazmat.2020.123496.

Wekerle, C., Wang, Q., von Appen, W.-J., Danilov, S., Schourup-Kristensen, V., Jung, T., 2017. Eddy-resolving simulation of the Atlantic water circulation in the Fram Strait

with focus on the seasonal cycle. J. Geophys. Res. Oceans 122, 8385–8405. https://doi.org/10.1002/2017JC012974.

Wekerle, C., Krumpen, T., Dinter, T., von Appen, W.-J., Iversen, M.H., Salter, I., 2018. Properties of sediment trap catchment areas in Fram Strait: results from Lagrangian modeling and remote sensing. Front. Mar. Sci. 5, 407. https://doi.org/10.3389/fmars.2018.00407.

Yakushev, E., Gebruk, A., Osadchiev, A., Pakhomova, S., Lusher, A., Berezina, A., van Bavel, B., Vorozheikina, E., Chernykh, D., Kolbasova, G., Razgon, I., Semiletov, I., 2021. Microplastics distribution in the Eurasian Arctic is affected by Atlantic waters and Siberian rivers. Communications Earth & Environment 2, 23. https://doi.org/10.1038/s43247-021-00091-0.